Characterization of some optical and physical properties of As$_{11.2}$S$_{48.0}$Sb$_{28.8}$Te$_{12.0}$ and As$_{20.8}$S$_{48.0}$Sb$_{19.2}$Te$_{12.0}$ nanostructured polycrystalline semiconductors

O. Iaseniuc[*], M. Iovu
Institute of Applied Physics, Str. Academiei 5, MD-2028 Chisinau, R. Moldova

This work presents the characterization of As-S-Sb-Te nanostructured polycrystalline semiconductors by X-ray fluorescence (XRF), X-ray diffraction (XRD), electron microscopy (SEM), optical as well as photoelectric methods. The XRD patterns have been shown the presence of amorphous and nanocrystalline phases with the main structural units As$_2$S$_3$, Sb$_2$S$_3$ and Sb$_2$Te$_3$. The IR transmission spectra show a high transparence just with a single weak absorption band about v=2340 cm^{-1} caused of the presence of H$_2$S impurity. It was also observed that for the alloys of As$_{11.2}$S$_{48.0}$Sb$_{28.8}$Te$_{12.0}$ and As$_{20.8}$S$_{48.0}$Sb$_{19.2}$Te$_{12.0}$, with an increase in the number of As atoms, the transmission in the IR region also increase. The maximum of steady-state photoconductivity for both materials, measured in the linear portion of I-V characteristics, is situated around λ=0.96 μm.

1. Introduction

Chalcogenide glasses have attracted much attention over the years due to their technological applications, infrared optical elements, as materials for image creation and storage of information, acousto-optic and memory switching elements [1, 2]. As$_2$S$_3$, As$_2$Se$_3$, Sb$_2$Te$_3$, and Sb$_2$S$_3$ and its ternary and quaternary compounds are the most intensively studied chalcogenide glasses because of its ease of formation, its excellent infrared transmission and its resistance to atmospheric conditions and chemical stability. Even though As and Sb belong to the same group of the periodic table, As$_2$S$_3$, As$_2$Te$_3$, and Sb$_2$S$_3$ do not display the same glass forming tendency [3]. Addition of As$_2$S$_3$ to Sb$_2$S$_3$ enhances the glass forming ability and glasses in the mixed As-S-Sb system can be formed [4].

The three-dimensional network of As$_2$S$_3$ glassy is built of trigonal pyramidal units AsS$_{3/2}$, which are interconnected through As-S-As bridges. The basic structural units of Sb$_2$S$_3$ are the trigonal pyramidal arrangement SbS$_{3/2}$ bonded to each other by S atoms [4]. The crystal structure of Sb$_2$Te$_3$ crystals with the band gap E_g=1.37 eV exhibits the layered atomic arrangement in the rhombohedral structure which consists of three quintuplet layers (QLs) and each quintuplet layer contain five atoms in the order of Te^1-Sb-Te^2-Sb-Te^1 [5, 6]. Some structural, thermoelectric and optical properties of Sb$_2$Te$_3$ and Sb$_2$S$_3$ (E_g=2.15 eV) are reported in [6]. Some photoelectric properties of (Sb$_{15}$As$_{30}$Se$_{55}$)$_{100-x}$Te$_x$ (0≤x≤12.5 at.%) thin films were investigated in [7]. It was shown that with increasing of Te concentration in the alloys, the maximum of photoconductivity is shifted toward the red region of the spectra from 800 nm to 950 nm.

It is well known that semiconductors containing As and S elements are high photosensitive amorphous materials, and are widely used for recording media of optical information. On the other hand, semiconductors containing Sb and Te elements are well known as "ovonic" materials for volatile memory. This work reports some experimental results concerning

---

the structural, optical and photovoltaic characterization of vitreous and polycrystalline semiconductors containing the As, S, Sb, Te elements ($As_{11.2}S_{48.0}Sb_{28.8}Te_{12.0}$, and $As_{20.8}S_{48.0}Sb_{19.2}Te_{12.0}$) in order to combine these two advantages using a single compositions. Moreover the investigations in this direction will be continued.

2. Experimental

The polycrystalline semiconductors $As_{11.2}S_{48.0}Sb_{28.8}Te_{12.0}$ and $As_{20.8}S_{48.0}Sb_{19.2}Te_{12.0}$ were prepared from the elements of *6N* purity (As, Sb, S, Te) by conventional melt quenching method. Initial chemical elements were placed and mixed in quartz ampoules, which then were evacuated up to pressure of $P\sim10^{-5}$ Torr and sealed. At last, the mixtures were melted at 850-900 ^{o}C in rocking furnace during 10 hours for homogenization, and then quenched at the room temperature. The X-ray diffraction (XRD) measurements were performed by DRON-UM1 diffractometer with *Fe-Kα* radiation (λ=1.936 Å), with *Mn* filter by *θ/2θ* scanning method. The samples also were characterized by X-ray fluorescence analyzer (XRF), which permits to estimate the presence of different chemical elements and phases in the investigated material. The surface morphology of all samples was examined by the scanning electron microscopy (SEM). For optical transmission spectra measurements the Spectrum 100 FTIR Spectrometer (PerkinElmer) ($v = 7800\div650$ cm^{-1}, λ=15$\div$2.5 μm) was used. The experimental samples for photoelectric measurements have a coplanar configuration with two Ag-electrodes superimposed at the surface at the distance of about 0.1 cm. The dark current and under illumination, and the spectral distribution of stationary photocurrent *Iph=f(λ)* was registered in the constant current conditions using the monochromator SPM-2 and the electrometer amplifier BK-70, with the error less than $\pm$ 1.0 %. All experiments were performed at room temperature ($T\approx$20 ^{0}C).

3. Results and discussion

3.1. XRF and SEM results

The XRF represents a device which allows registering the presence of different chemical elements from the periodic table and can estimate its quantity. The energetic spectrums of the emitted K_α or K_β, radiation are unique for individual chemical element, and the intensity of the emitted radiation correlate with the concentration of the specific atoms in the analyzed materials.

As an example in the Table 1 and Fig. 1 are shown the experimental XRF results and SEM images obtained for the investigated $As_{20.8}S_{48.0}Sb_{19.2}Te_{12.0}$ and $As_{11.2}S_{48.0}Sb_{28.8}Te_{12.0}$ nanostructured semiconductors.

Table 1. XRF results of $As_{20.8}S_{48.0}Sb_{19.2}Te_{12.0}$ and $As_{11.2}S_{48.0}Sb_{28.8}Te_{12.0}$ compositions.

$As_{20.8}S_{48.0}Sb_{19.2}Te_{12.0}$			$As_{11.2}S_{48.0}Sb_{28.8}Te_{12.0}$		
Element	Conc. mg/cm^2	Mole (%)	Element	Conc. mg/cm^2	Mole (%)
As	7.96	7.35	As	16.54	14.61
Sb	52.10	29.61	Sb	35.96	19.54
S	25.61	55.27	S	26.68	55.05
Te	14.32	7.77	Te	20.82	10.80
Total	100 %	100 %	Total	100 %	100 %
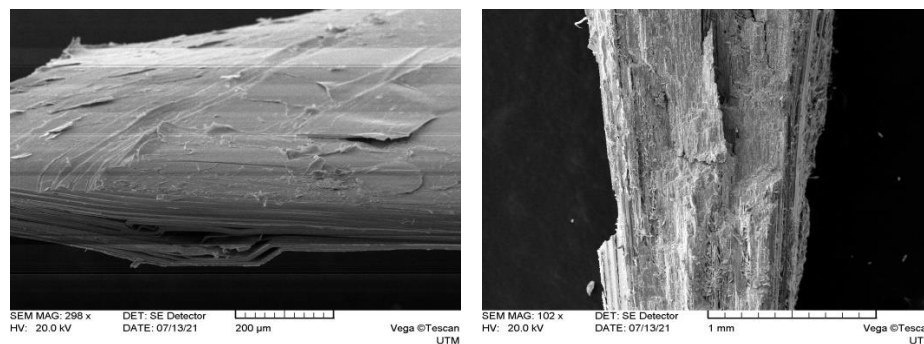
Fig. 1. SEM images of As$_{20.8}$S$_{48.0}$Sb$_{19.2}$Te$_{12.0}$ and As$_{11.2}$S$_{48.0}$Sb$_{28.8}$Te$_{12.0}$ compositions.

The XRF results from the Table 1 show the presence of all chemical elements in the investigated samples.

The SEM images of the As$_{20.8}$S$_{48.0}$Sb$_{19.2}$Te$_{12.0}$ and As$_{11.2}$S$_{48.0}$Sb$_{28.8}$Te$_{12.0}$ compositions indicate on the layered structure of the nanostructured semiconductor.

3.2. X-ray diffraction patterns

Fig. 2 represents the X-ray diffraction patterns for the As$_{20.8}$S$_{48.0}$Sb$_{19.2}$Te$_{12.0}$ and As$_{11.2}$S$_{48.0}$Sb$_{28.8}$Te$_{12.0}$ powders. For the As$_{20.8}$S$_{48.0}$Sb$_{19.2}$Te$_{12.0}$ sample the main peaks were identified with interplanar distance about d=3.21 Å ($2\theta\approx35^0$) for Sb$_2$S$_3$, d=2.35-2.37 Å ($2\theta\approx49^0$–48^0) for Sb$_2$Te$_3$, and the maximum peak d=3.157 Å ($2\theta\approx34,4^0$) for Sb$_2$Te$_3$ units. The peaks with interplanar distances d=3.23 Å ($2\theta\approx34^0$), d=3.13 Å ($2\theta\approx35^0$), d=2.1 Å ($2\theta\approx55^0$) and d=2.33 Å ($2\theta\approx49^0$), d=2.1 Å ($2\theta\approx55^0$) and d=2.33 Å($2\theta\approx49^0$) are also detected for Sb$_2$S$_3$ units. It is also assumed that some peaks may overlap for Sb$_2$S$_3$ and Sb$_2$Te$_3$.

The As$_{11.2}$S$_{48.0}$Sb$_{28.8}$Te$_{12.0}$ sample was found to be amorphous with some microcrystalline phases. The peaks on the X-ray diffraction pattern for above mentioned sample are more pronounced, that indicate on the presence Sb$_2$S$_3$ and Sb$_2$Te$_3$ microcrystalline incorporations. But the peak with interplanar distance d=5.72 Å is not identified yet (it will be investigated).
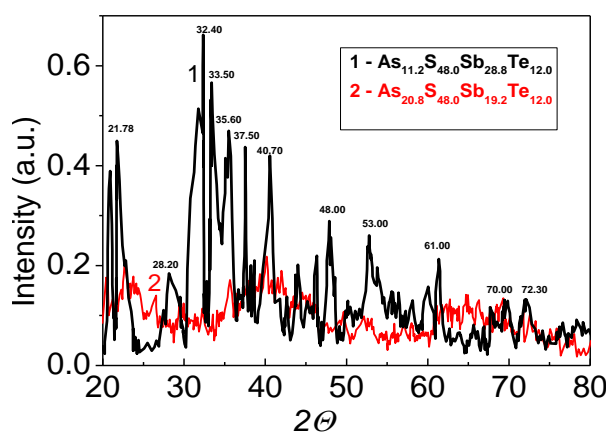
Fig. 2. XRD patterns of As$_{11.2}$S$_{48.0}$Sb$_{28.8}$Te$_{12.0}$ and As$_{20.8}$S$_{48.0}$Sb$_{19.2}$Te$_{12.0}$ samples.

According to the [7] the monocrystals Sb$_2$Te$_3$, Sb$_2$Se$_3$ and Sb$_2$S$_3$ are well-known layered bulk structures with Van Der Vals interactions. It was shown, that in the crystal structures of Sb$_2$X$_3$ (where X=S, Se, Te) each Sb atom is surrounded by six X atoms, and each X atoms encompassed by four Sb atoms. The bond lengths $d_{1,2}$ and $d_{3,4}$ were determined to be 2.66/2.59 Å and 2.56/4.94 Å for Sb$_2$S$_3$ monolayer, and 2.95/3.13 Å and 2.99/3.02 Å for Sb$_2$Te$_3$ monolayer,

respectively. Some structural investigations of the chalcogenide glasses in the Sb_2S_3-As_2S_3-Sb_2Te_3 and $(As_2S_3)_{1-x}(Sb_2S_3)_x$ system was reported in [8-10].

3.3. Optical properties

Fig. 3 illustrates the absorbance calculated from the reflectance spectra using expression (1) for the bulk $As_{11.2}S_{48.0}Sb_{28.8}Te_{12.0}$ and $As_{20.8}S_{48.0}Sb_{19.2}Te_{12.0}$ nanostructured semiconductors in the NIR spectral range.

$$A = 2 - \log_{10}(1 - R(\%)) \tag{1}$$

It was observed, that with an increase of Sb and decreasing of As contents in the alloys the reflectance raise.
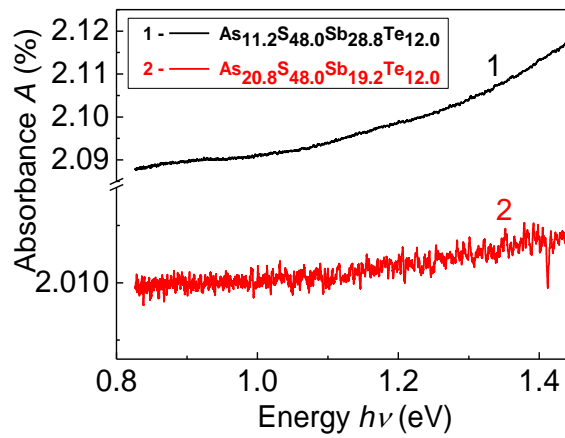
Fig. 3. Absorbance of $As_{11.2}S_{48.0}Sb_{28.8}Te_{12.0}$ (1) and $As_{20.8}S_{48.0}Sb_{19.2}Te_{12.0}$ (2) nanostructured semiconductors.

Fig. 4 represents the transmission spectra $T=f(\lambda)$ in the IR region for the above mentioned samples. It can be seen that for both materials, transparency in the IR region is high and decreases at short-wave numbers in the phonon region of the spectra.
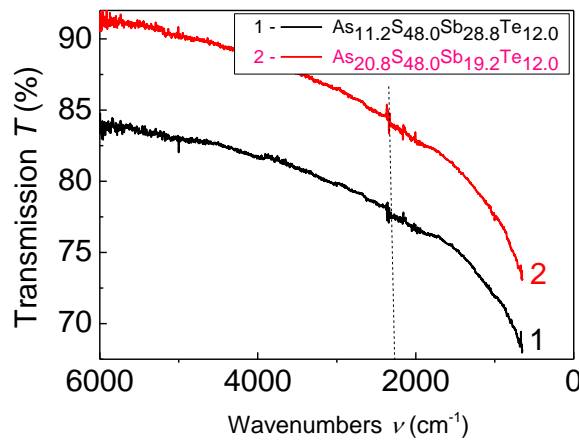
Fig. 4. Transmission spectra $T=f(v)$ in the IR region of $As_{11.2}S_{48.0}Sb_{28.8}Te_{12.0}$ (1) and $As_{20.8}S_{48.0}Sb_{19.2}Te_{12.0}$ (2) nanostructured semiconductors.

3.4. Photoelectric properties

Fig. 5 and 6 represent the spectral distribution of the stationary photocurrent $I_{phc}=f(\lambda)$ for $As_{11.2}S_{48.0}Sb_{28.8}Te_{12.0}$ and $As_{20.8}S_{48.0}Sb_{19.2}Te_{12.0}$ nanostructured semiconductors at different applied voltages (U=10÷300 V) and in the wavelength range from 0.4÷1.3μm. In the all photocurrent spectral distributions we have observed a maximum photosensitivity situated around λ=0.96 μm.
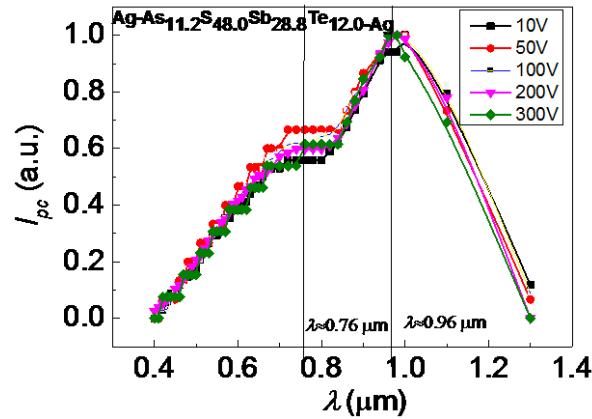
Fig. 5. Spectral distribution of the stationary photocurrent $I_{phc}=f(\lambda)$ of $As_{11.2}S_{48.0}Sb_{28.8}Te_{12.0}$ and $As_{20.8}S_{48.0}Sb_{19.2}Te_{12.0}$ nanostructured semiconductors at different applied voltages.
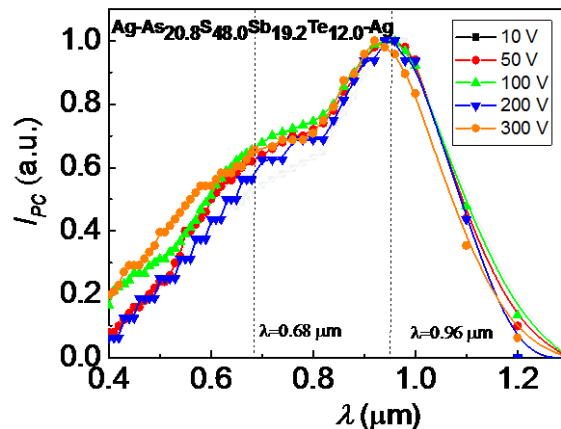
Fig. 6. Spectral distribution of the stationary photocurrent $I_{phc}=f(\lambda)$ of $As_{11.2}S_{48.0}Sb_{28.8}Te_{12.0}$ and $As_{20.8}S_{48.0}Sb_{19.2}Te_{12.0}$ nanostructured semiconductors at different applied voltages.

Besides that, in these spectral distributions of the stationary photocurrent an additional shoulder appears around λ=0.76 μm ($h\nu\approx$1.63 eV) for $As_{11.2}S_{48.0}Sb_{28.8}Te_{12.0}$ and around λ=0.68 μm ($h\nu\approx$1.82 eV) for the $As_{20.8}S_{48.0}Sb_{19.2}Te_{12.0}$ semiconductors. The presence of second maximum in the spectral distribution of the photocurrent, taking into account the X-ray diffraction data, can be associated with the presence in the alloys of some nanostructured Sb_2S_3 and Sb_2Te_3 units.

Usually, the photocurrent I_{phc} in semiconductor materials is proportional to the absorption coefficient α, quantum efficiency β, mobility μ, and life time τ:

$$I_{phc} \sim \frac{1-e^{-\alpha d}}{d}\beta\mu\tau \tag{2}$$

In the weak absorption region (long wave region), the photocurrent I_{phc} is described by the absorption coefficient α:

$$I_{phc} \sim \beta\alpha\mu\tau \qquad (3)$$

Low values of the photocurrent in the high-energy region are caused by an increase in the rate of surface recombination.

For estimation of the band gap E_g values, both, the spectra of the photocurrent and the Moss rule were used as in the case of amorphous $(As_4S_3Se_3)_{1-X}Sn_X$ and $Ge_xAs_xSe_{1-2X}$ thin films [11]. In accordance with this, the band gap takes the value of the wavelength at which the photocurrent fall down to a half of its maximum value:

$$E_g{}^{pc} = \frac{1.24}{\lambda_{1/2}} \qquad (4)$$

The estimated value for $As_{11.2}S_{48.0}Sb_{28.8}Te_{12.0}$ and $As_{20.8}S_{48.0}Sb_{19.2}Te_{12.0}$ samples is about $E_g=1.41$ eV and is close to that of $E_g=1.37$ eV for Sb_2Te_3 single monolayer [6].

It is well known the photoelectric properties allow obtaining information about the generation and recombination processes in semiconductors [12-14]. The respective measurements were carried out at different applied voltage, in the linear current-voltage (*I-V*) characteristics.

The *I-V* characteristics for $As_{11.2}S_{48.0}Sb_{28.8}Te_{12.0}$ and $As_{20.8}S_{48.0}Sb_{19.2}Te_{12.0}$ nanostructured semiconductors in the dark and under illumination in the range of applied voltages $U=10\div300$ V ($E=10^2\div3\cdot10^3$ V/cm) are illustrated in the Fig. 7. As can be seen from that figure the *I-V* characteristics have linear behavior.
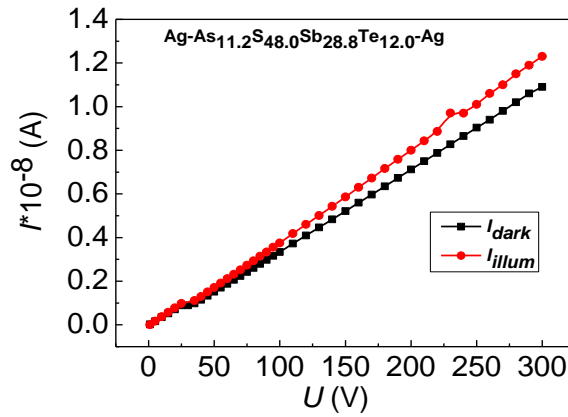
Fig. 7. I-V characteristics of $As_{11.2}S_{48.0}Sb_{28.8}Te_{12.0}$ nanostructured semiconductors in the dark and under illumination.

Fig. 8 shows the *I-V* characteristics of the studied materials in the dark and under illumination at $\lambda=0.96\mu m$, $h\nu\approx1.3$ eV, where materials show the maximum sensitivity.
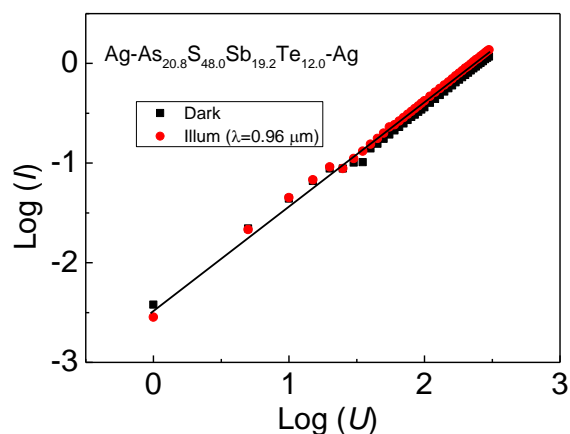
Fig. 8. I-V characteristics of As$_{20.8}$S$_{48.0}$Sb$_{19.2}$Te$_{12.0}$ nanostructured semiconductors in the dark and under illumination at λ=0.96μm.

From that dependence we can see that with an increase of applied voltage the photosensitivity of investigated samples at the maximum value of the photocurrent in the spectral distribution also increases.

4. Conclusions

Some nanostructured layered semiconductors of As-S-Sb-Te system were investigated by XRF, XRD, SEM as well as by optical and photoelectric methods.

The X-ray diffraction patterns and SEM images of studied materials show the presence of amorphous and nanocrystalline phases with the main structural units AsS_3, Sb_2S_3 and Sb_2Te_3.

The transmission spectra in the IR region of wave numbers v=6000 ÷ 1000 cm^{-1} show a high transparence in the studied materials.

The spectral distribution of the stationary photocurrent I_{pc}=$f(\lambda)$ both for As$_{11.2}$S$_{48.0}$Sb$_{28.8}$Te$_{12.0}$ and As$_{20.8}$S$_{48.0}$Sb$_{19.2}$Te$_{12.0}$ nanostructured semiconductors at different applied voltages shows a maximum situated around λ=0.96 μm (hv≈1.3 eV) and an additional shoulder situated around λ=0.76 μm (for As$_{11.2}$S$_{48.0}$Sb$_{28.8}$Te$_{12.0}$) and around λ=0.68 μm (for As$_{20.8}$S$_{48.0}$Sb$_{19.2}$Te$_{12.0}$).

The estimated value of the band gap value found by the photoelectric method for the above mentioned studied samples is about E_g=1.41 eV.

References

[1] A. B. Seddon, J. Non-Cryst. Solids 184, 44 (1995); https://doi.org/10.1016/0022-3093(94)00686-5
[2] I. Blonskyi, V. Kadan, O. Shpotyuk, M. Iovu, et al., Applied Physics B 104, 1 (2011); https://doi.org/10.1007/s00340-011-4390-x

[3] L. Cervinka, A. J. Hruby, Non-Cryst. Solids 48, 231 (1982); https://doi.org/10.1016/0022-3093(82)90164-8

[4] E. I. Kamitsos, J. A. Kapoutsis, I. P. Culeac, M. S.Iovu, J. Phys. Chem. B, 101, 11061 (1997); https://doi.org/10.1021/jp972348v

[5] R. Indu, R. Sumesh, P. Jena Rudra, L. Archana, AIP Conf. Proc. 2100, 020070 (2019)

[6] A. Bafekry, B. Mortazavi, M. Faraji, et al., Journal Scientific Reports 11, 10366 (2021); https://doi.org/10.1038/s41598-021-89944-4

[7] K. A. Aly, A. M. Abouschly, A. A. Othman, J. Non-Cryst. Solids 354, 909 (2008).

[8] K. N'dri, V. Coulibaly, V. Houphouet-Boigny, C. Jumas, J. of Ovonic Research 9, 113 (2013).

[9] F. Sava, J. of Optoelectronics and Advanced Materials 3, 425 (2001).

[10] A. Stronski, L. Revulska, L. Shportko, et al., Functional Materials 27, 315 (2020).

[11] O. Iaseniuc, M. Iovu, Rom. Rep. in Phys. 69, 505 (2017).

[12] A. Rose, Concepts in photoconductivity and allied problems, Interscience Publishers John Wiley & Sons, New York - London (1963).

[13] S. M. Ravkin, Photoelectrical phenomena in semiconductors, Fizmatgiz Publishers, Moskow, in Russian, 496 p. (1963).

[14] M. Popescu, A. Andriesh, V. Ciumash, M. Iovu, S. Shutov, D. Tsyiuleanu, Physics of chalcogenide glasses, Ed.Bucuresti, Stiinta, in Romanian, 487 (1996).